JPE 19-4-1

https://doi.org/10.6113/JPE.2019.19.4.835
ISSN(Print): 1598-2092 / ISSN(Online): 2093-4718

# Augmentation of Fractional-Order PI Controller with Nonlinear Error-Modulator for Enhancing Robustness of DC-DC Boost Converters

Omer Saleem†, Mohsin Rizwan*, Ahmad Khizar*, and Muaaz Ahmad**

*Dept. of Mechatronics and Control Eng., University of Engineering and Technology (UET), Lahore, Pakistan
†,**Dept. of Electrical Eng., National University of Computer and Emerging Sciences (NUCES), Lahore, Pakistan

**Abstract**

This paper presents a robust-optimal control strategy to improve the output-voltage error-tracking and control capability of a DC-DC boost converter. The proposed strategy employs an optimized Fractional-order Proportional-Integral (FoPI) controller that serves to eliminate oscillations, overshoots, undershoots and steady-state fluctuations. In order to significantly improve the error convergence-rate during a transient response, the FoPI controller is augmented with a pre-stage nonlinear error-modulator. The modulator combines the variations in the error and error-derivative via the signed-distance method. Then it feeds the aggregated-signal to a smooth sigmoidal control surface constituting an optimized hyperbolic secant function. The error-derivative is evaluated by measuring the output-capacitor current in order to compensate the hysteresis effect rendered by the parasitic impedances. The resulting modulated-signal is fed to the FoPI controller. The fixed controller parameters are meta-heuristically selected via a Particle-Swarm-Optimization (PSO) algorithm. The proposed control scheme exhibits rapid transits with improved damping in its response which aids in efficiently rejecting external disturbances such as load-transients and input-fluctuations. The superior robustness and time-optimality of the proposed control strategy is validated via experimental results.

**Key words:** Boost converter, Capacitor-current, Error modulation, Fractional-order PI controller, Hyperbolic secant function, Particle swarm optimization

## I. INTRODUCTION

Interest in DC-DC switching power electronic converters has gained a lot of momentum due to their enhanced conversion efficiency [1]. Owing to their low production cost, small size, and large power output, boost converters are widely used as the main constituent of the electrical energy conversion systems of hybrid electric vehicles, wind-energy generators, solar photovoltaic generators, etc. [2]. Boost converters increase the average value (DC component) of the voltage to a desired level using a high-frequency switching transistor [3]. Maintaining the robustness and optimality of a boost converter's output-voltage regulation capability under the influence of load-transients and input-voltage fluctuations poses a great challenge for research engineers [4], [5].

Voltage regulation can be optimized by utilizing a well-postulated closed-loop feedback control scheme [6]-[9]. One of the most widely used model-free voltage-regulation schemes is the proportional-integral-derivative (PID) controller [10], [11]. It is a simple and stable controller that provides a reliable control effort based on the weighted sum of the error-dynamics [12]. The integral controller aids in eliminating steady-state errors and offers reasonable damping to attenuate overshoots, undershoots and persistent oscillations at the expense of the systems convergence rate. Meanwhile, the derivative controller improves the transitional times but injects high- frequency noise into the response. Hence, the derivative control term is normally neglected in boost converter controllers [13]. PI controllers are unable to compensate unprecedented state-variations occurring in complex dynamical systems. Fuzzy

Manuscript received Sep. 21, 2018; accepted Mar. 8, 2019
Recommended for publication by Associate Editor Seongjun Lee.
†Corresponding Author: omer.saleem@nu.edu.pk
Tel: +92-111-128-128 (Ext. 364), NUCES
*Dept. Mechatron. & Contr. Eng., Univ. Eng. Tech. (UET), Pakistan
**Dept. Electr. Eng., National Univ. Comp. Emerg. Sci. (NUCES), Pakistan

controllers are difficult to synthesize because they require a lot of training data and elaborate logical rules to deliver robust control decisions [14], [15]. Sliding-mode controllers offer a robust control effort [16]-[18]. However, they inject chattering in the response and expend a lot of control energy [19]. The augmentation of integer-order PI controllers with fractional calculus enables the control strategy to compensate for the effects of the un-modeled intrinsic nonlinearities associated with real-world dynamical systems [20], [21]. In this case, the conventional integral operator is replaced by a fractional-order integral operator [22]. The addition of a fractional-order parameter, along with the two PI controller gains, increases the degree-of-freedom and design flexibility of the controller [23]. However, even an optimized FoPI controller can exhibit long transient recovery times and poor robustness against exogenous disturbances owing to its lack of knowledge regarding the error-derivative information [24]. Slow transitions and poor disturbance rejection capability deteriorate the efficiency of the power conversion system.

The novel contribution of this article is the methodic synthesis of a robust and time-optimal control scheme for boost-converter based power management systems. The proposed strategy primarily employs an FoPI controller. In order to improve the transient response while maintaining minimal oscillations and negligible steady-state error, the FoPI controller is augmented with a pre-stage error-modulator. The modulator aggregates the incoming instantaneous signals of the error and error-derivative using the Signed Distance Method (SDM). Then it feeds them to a smooth sigmoidal control surface. The sigmoidal surface comprises a Signed Hyperbolic Secant Function (SHSF) that depends on variations in the aggregated-signal. The SHSF reduces the control effort for very small error variations in order to maintain reasonable damping and eliminate the steady-state error. When error enlarges, the modulated control signal is proportionally amplified in order to improve the disturbance-rejection capability and to offer minimum-time transient recovery. Under extremely large error-dynamics, the aggregated output is bounded within pre-defined limits to prevent the control input signal from getting saturated. Consequently, the response exhibits rapid transits with minimum oscillations and reasonable damping. The proposed augmentation enables the controller to effectively reject and recover from the influence of load-transients and input fluctuations in minimum time with minimal overshoot. In this research, the error-derivative is not computed directly using the differentiation of the incoming error signals. Instead, it is evaluated indirectly by measuring variations in the output-capacitor current [25]. This modification suppresses the hysteresis effect caused by parasitic impedances. Eventually, the derived modulated signal is fed to the fixed-gain FoPI controller, which generates appropriate correction effort to maintain reasonable damping and to nullify the steady-state fluctuations. The PI controller gains, the exponent of the fractional integral-operator, and the hyper-parameters of the SHSF are meta-heuristically selected offline using a particle swarm optimization (PSO) algorithm [26], [27]. The proposed technique is simple and robust. It does not result in a recursive computational burden. Thus, it is completely practicable. The performance of the proposed control scheme is benchmarked against conventional fixed-gain PI and FoPI controllers and its efficacy is justified via experimental results.

The rest of this paper is organized as follows. Section II presents details of the experimental setup of the boost converter. The theoretical background and construction of the FoPI controller are presented in section III. Integration of the proposed nonlinear error-modulation scheme with the FoPI controller is presented in section IV. The optimization process of the controller parameters is explained in section V. Experimental tests and a comparative performance assessment of the results are presented in section VI. The paper is concluded in Section VII.

## II. System Description

A circuit schematic of a conventional DC-DC boost convertor is shown in Fig. 1. The circuit is operated in the continuous conduction mode (CCM) due to the changes occurring in its configuration when the transistor turns on and off in each switching period [28]. The output voltage is regulated by dynamically adjusting the duty cycle $d$ applied at the gate of the switching transistor ($Q$). The output voltage ($v_o$) of boost converter is given by Equ. (1).

$$v_o = \left(\frac{1}{1-d}\right) v_{in} \tag{1}$$

such that:

$$d = \frac{t_{on}}{t_{on} + t_{off}} \tag{2}$$

where $t_{on}$ and $t_{off}$ are the on-time and off-time of the switching transistor. The feedback controller adaptively adjusts the duty-cycle of the switching period in order to accurately track the reference value of $v_o$, even in the presence of load variations or input fluctuations. The inductor ($L$) in the input circuit removes abrupt fluctuations occurring in $v_{in}$. A large capacitor ($C$) is used in the output circuit so that its time-constant is higher than the switching period. When $Q$ is turned on, the diode gets reverse-biased. Hence, the inductor gets decoupled from the output circuit. Consequently, during this time, the inductor charges and stores magnetic energy. Meanwhile, the output capacitor discharges the supply current to the load resistor ($R_L$) using the energy stored in it during the previous off-state of $Q$. During the off-time of the switch, the diode gets forward biased. Thus, it couples the charged inductor with the rest of the circuit. The voltage polarity of the charged inductor reverses and it begins to discharge. Together, the actual $v_{in}$ source and the discharging inductor serially supply current to the resistor-capacitor combination in the output circuit.

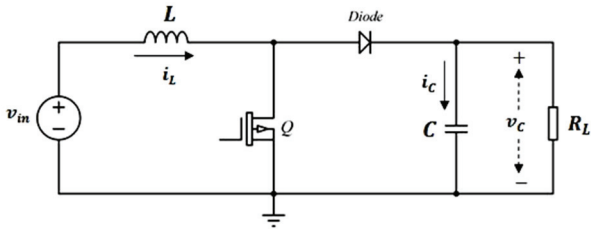


Fig. 1. Boost converter circuit schematic.

The capacitor continues to charge during this time. Before the inductor can significantly discharge, the switch $Q$ turns on again. The small-signal state-space model of the DC-DC boost converter is acquired via the averaging technique [29]. The model describes the variations in the state-trajectories and dynamics of the system about the steady-state operating point. The generalized linear model of the boost converter is given by Eqns. (3) and (4).

$$\dot{x}(t) = \boldsymbol{A}x(t) + \boldsymbol{B_1}v_{in}(t) + \boldsymbol{B_2}d(t) \tag{3}$$

$$v_o(t) = \boldsymbol{C}x(t) + \boldsymbol{F}d(t) \tag{4}$$

where *x(t)* is the state-vector, *d(t)* is the instantaneous value of the duty-cycle and is taken as the control input, *A* is the system matrix, $B_1$ and $B_2$ are the input matrix, *C* is the output matrix, and *F* is the feed-forward matrix. The state-vector of the boost converter is given by Equ. (5).

$$x(t) = [i_L(t) \quad v_o(t)]^T \tag{5}$$

The matrices *A*, $B_1$, $B_2$, *C* and *F* of the boost converter's state-space model are identified in Equ. (6), [30].

$$\begin{aligned} A &= \begin{bmatrix} -\left(\frac{r_L}{L} + \frac{r_c||R_L}{L}(1-D)\right) & -\frac{R_L}{L(R_L+r_c)}(1-D) \\ \frac{R_L}{C(R_L+r_c)}(1-D) & -\frac{1}{C(R_L+r_c)} \end{bmatrix}, \\ B_1 &= \begin{bmatrix} \frac{1}{L} \\ 0 \end{bmatrix}, \qquad B_2 = \begin{bmatrix} \frac{R_L}{L(R_L+r_c)}V_o \\ -\frac{R_L}{C(R_L+r_c)}I_L \end{bmatrix}, \\ C &= \begin{bmatrix} 0 & \frac{R_L}{R_L+r_c} \end{bmatrix}, \qquad F = 0 \end{aligned} \tag{6}$$

The state variables and the control input *d(t)* are characterized as small-signal AC perturbations occurring in the steady-state (or nominal) values of the inductor current ($I_L$), output voltage ($V_o$), and duty-cycle (*D*). The nominal value of *D* is evaluated using the expression in Equ. (7).

$$D = 1 - \frac{v_{in}}{v_0} \tag{7}$$

The design parameters mentioned in Equ. 6 are clearly identified in Table I. The identified state space model is used to deduce the averaged small signal model of the boost converter. The second order small signal model is given by Equ. (8), [28].

$$\frac{v_o(s)}{d(s)} = \frac{v_{in}}{(1-D)^2}\left(1 - s\frac{L_\varepsilon}{R_L}\right)\left(\frac{1 + sr_cC}{CL_\varepsilon\left(s^2 + s\left(\frac{1}{R_LC} + \frac{r_c}{L_\varepsilon}\right) + \frac{1}{CL_\varepsilon}\right)}\right) \tag{8}$$

TABLE I
BOOST CONVERTER CIRCUIT DESIGN PARAMETERS

| Parameters | Symbol | Values |
|---|---|---|
| Load-resistor | $R_L$ | 10 Ω |
| Inductor | $L$ | 120 µH |
| Output capacitor | $C$ | 330 µF |
| Equivalent-series-resistance of capacitor | $r_c$ | 0.17 Ω |
| Equivalent-series-resistance of inductor | $r_L$ | 0.12 Ω |
| Input voltage | $v_{in}$ | 24.0 V |
| Reference output voltage | $v_{ref}$ | 30.0 V |
| Maximum output Power | $P_{out}$ | 250 W |
| Maximum conversion efficiency | $\eta$ | 92% |

where *s* is the Laplace operator, and $L_\varepsilon = {}^{L}/_{(1-D)^2}$.

## III. FRACTIONAL ORDER PROPORTIONAL-INTEGRAL CONTROLLER

The proportional-integral (PI) controller is model-free control scheme that is widely used due to its simplicity and robustness [31]. The proportional control term depends on the instantaneous value of error and applies appropriate correctional effort to converge the response to the reference value.

The integral term depends on the accumulated value of the error in $v_o$. This introduces a closed-loop pole at the origin in order to improve the damping of the system. Hence, under transient conditions, the integral controller manipulates the magnitude of the accumulated error to reset and saturate the error response to a zero value. Consequently, it effectively damps both oscillations and overshoots, and eliminates steady-state fluctuations in the system's response. As discussed earlier, the PI controller is the weighted combination of the error and the numerical-integral of recent errors. The weightages of these error dynamics are denoted as the proportional gain ($k_P$) and the integral gain ($k_I$). The integer-order PI control law is given by Equ. (9).

$$d(t) = k_P.e(t) + k_I.\left(\int_0^T e(\tau)d\tau\right) \tag{9}$$

such that:

$$e(t) = v_o(t) - v_{ref}(t) \tag{10}$$

Fractional calculus is a branch of mathematics that serves to realize, model and control physical systems exhibiting non-integer fractional-order characteristics [32]. Fractional-order systems are identified via fractional-order differential equations. These equations mainly deal with differential and integral operators having real number powers. The fractional operator is denoted by $G^\beta$, where $\beta$ is the positive and real-numbered exponent of the operator. The fundamentals of fractional calculus are described by three common definitions provided by Riemann-Liouville, Gruunwald-Letnikov, and

Caputo in [33]. These definitions are outlined in Eqns. (11)-(13).

$$G^{\beta}f(t) = \frac{1}{\Gamma(n-\beta)}\frac{d^n}{dt^n}\int_a^t \frac{f(\tau)}{(t-\tau)^{\beta-n+1}}d\tau \tag{11}$$

where Γ(x) represent the Euler gamma function, n is the integer number, and n-1 < β < n.

$$G^{\beta}f(t) = \lim_{h\to 0}\frac{1}{h^{\beta}}\sum_{j=0}^{(t-a)/h}(-1)^j\binom{\beta}{j}f(t-jh) \tag{12}$$

where $\binom{\beta}{j} = \Gamma(\beta+1)/\Gamma(j+1)\,\Gamma(\beta-j+1)$, and $h$ is the step-size.

$$G^{\beta}f(t) = \frac{1}{\Gamma(\beta-n)}\int_a^t \frac{f^n(\tau)}{(t-\tau)^{\beta-n+1}}d\tau \tag{13}$$

The conventional PI controller is transformed into the FoPI controller using the definitions outlined above. The FoPI control law, in the time-domain, is given by Equ. (14), [34].

$$d(t) = k_P.e(t) + k_I.\left(G^{-\beta}e(t)\right) \tag{14}$$

The FoPI controller is a generalized form of the integer-order PI controller. If the value of $\beta$ is set to zero, the control law is reduced to a generic proportional controller. If $\beta$ is selected to be one, the control law transforms into a conventional fixed-gain PI controller. With the introduction of the new hyper-parameter $\beta$, the three-parameters control law tends to improve the degrees of freedom and design flexibility of the controller. If optimized properly, the FoPI control law offers enhanced robustness against exogenous disturbances when compared to the conventional PI controller. In this paper, the three fixed controller parameters of the FoPI control law are optimally tuned via a PSO algorithm. The generalized transfer function of the control law is given in Equ. (15).

$$C(s) = \frac{D(s)}{E(s)} = k_P + \frac{k_I}{s^{\beta}} \tag{15}$$

The term $s^{-\beta}$, in Equ. (15), has a fractional order that makes it difficult to implement. Hence, in this paper, the fractional integral operator is approximated using a 5th order Oustaloup's recursive filter for the practical implementation of a FoPI controller in a digital computer. The Oustaloup's approximation of $s^{\beta}$ is given by Equ. (16), [35].

$$s^{\beta} = \prod_{n=1}^{N}\frac{1+\frac{s}{\omega_{z,n}}}{1+\frac{s}{\omega_{p,n}}} \tag{16}$$

where $N$ is the number of zeros or poles. Normally, a large value of $N$ is selected so that the undulations in the gain and phase responses are avoided without significantly increasing the computational cost. The aforementioned approximation is valid for a frequency range between $[\omega_L; \omega_H]$. The frequencies of the poles and zeros are evaluated using Equ. (17).

$$\omega_{z,1} = \omega_L\sqrt{\rho}, \quad \omega_{p,n} = \omega_{z,n}\sigma, \quad \omega_{z,n+1} = \omega_{p,n}\rho \tag{17}$$

such that:

$$\sigma = \left(\frac{\omega_H}{\omega_L}\right)^{\frac{\beta}{N}}, \qquad \rho = \left(\frac{\omega_L}{\omega_H}\right)^{\frac{1-\beta}{N}}$$

The lower and upper translational frequencies of the filter are $\omega_L = 10^3$ rad/s and $\omega_H = 10^8$ rad/s, respectively. These frequencies are selected according to the study presented in [23].

## IV. Nonlinear Error Modulator

The duty-cycle adjustment commands generated by a conventional fixed-gain FoPI controller lack the ability to quickly compensate the nonlinear disturbances encountered by the system. Hence, in order to improve the time-optimality of the control scheme, the FoPI controller is augmented with a pre-stage error modulator. The modulator comprises a well-postulated nonlinear control surface that dynamically adjusts the signal being fed to the FoPI controller. This is based on instantaneous variations in the error and error-derivative of $v_o$. The derived modulated signal enhances the controller's ability to reject exogenous disturbances, modeling errors, and other intrinsic nonlinearities. The improved disturbance-compensation capability enables the controller to quickly recover from load or input transients with minimum oscillations.

Extensive research has been done to develop nonlinear gain adjustment mechanisms to modify the classical control schemes of complex dynamical systems. A state-dependent nonlinear self-tuning mechanism designed to dynamically update the controller gains was proposed in [36]. The controller lacked information regarding the error-dynamics. Hence, it demonstrates a slow convergence rate. The nonlinear gain adaptation scheme proposed in [37] depends only on the direction of the error-derivative and not its magnitude. This results in sluggishness in the response. The error-dependent sigmoidal functions proposed in [38] offer a smooth transition between subsequent controller gains while adjusting them with respect to variations in the error. However, these functions also lack information regarding the error-derivative, which prevents them from efficiently compensating rapid variations in the state dynamics.

It is well-known that the incorporation of an error-derivative term in the control law significantly improves the phase-margin of the controlled system [39]. This addition enhances the disturbance-attenuation capability and error- convergence rate of the response. However, its inclusion also has some drawbacks. The derivative operation unavoidably amplifies and injects high frequency noise into the system, which increases the fluctuations in the steady-state response. Optimal estimation of the error-derivative after every sampling interval puts a computational burden on the digital computer. Hence, a simple yet practicable approach to accurately estimate the error-derivative is to measure the current flowing through the output-capacitor of the converter $i_c$ in real-time. The output-capacitor is practically modeled according to Equ. (18).

$$\dot{v}_o(t) = L_c \frac{d^2 i_c(t)}{dt^2} + r_c \frac{d i_c(t)}{dt} + \frac{i_c(t)}{C} \quad (18)$$

where $L_c$ is the equivalent-series-inductance (ESL) and its value is 100 nH. DC-DC boost conversion is a regulation problem. Hence, the instantaneous value of $\dot{v}_o(t)$ is assumed to be equal to the error-derivative $\dot{e}(t)$. With this assumption in mind, the time-domain response of $i_c$ is given by Equ. (19).

$$i_c(t) \approx \frac{r_c}{r_c C - L_c}\left(e^{\frac{-t}{r_c C}} - e^{\frac{-r_c t}{L_c}}\right) C\dot{e}(t) \quad (19)$$

The expression in Equ. (19) clearly shows that $\dot{e}(t)$ is directly proportional to $i_c$. The utilization of $i_c$ offers following the benefits to the controlled system [40].

- It significantly improves the transient recovery response of the system, even in the presence of transient detection delays.
- It has an insignificant effect on the closed-loop bandwidth and stability of the system.
- It attenuates the hysteresis effect contributed by the parasitic impedances.
- It indirectly feeds the system with information regarding variations in the inductor-current and load-current.

Due to its advantages, the information regarding $i_c$ is included in the existing control law by combining its instantaneous values with those of *e(t)* using the Signed Distance Method (SDM). The SDM is a data-aggregation technique that is widely used in combining the input signals for single input fuzzy logic controllers [41]. Prior to their unification, the values of $i_c(t)$ and *e(t)* are normalized. Afterwards, they are aggregated using the expression given in Equ. (20), [42], [43].

$$q(t) = \frac{i_c(t) + \mu e(t)}{\sqrt{1+\mu^2}} \quad (20)$$

such that:

$$\mu = \frac{2k_I T_s}{k_I T_s - 2k_P} \quad (21)$$

where $T_s$ is the sampling time of the system. The value of $T_s$ used in this paper is 0.25 ms. The aggregated signal *q(t)* derived from the SDM is fed to the nonlinear control surface as its sole input variable. As discussed earlier, sigmoidal functions offer an effective control effort due to their smoothness, differentiability and roundness. Hence, in this paper, the Signed-Hyperbolic-Secant-Function (SHSF) is used as the nonlinear control surface. The characteristic waveform of the SHSF is given by Equ. (22).

$$f(t) = \alpha . sgn\big(q(t)\big) . sech\big(\gamma . q(t)\big) \quad (22)$$

where $sgn(.)$ is the sign function that extracts the sign of $q(t)$, $sech(.)$ is the nonlinear hyperbolic secant function, $\gamma$ is the variation-rate of the waveform, and $\alpha$ defines the upper and lower limits of the waveform. The hyper-parameters, $\gamma$ and $\alpha$, increase the flexibility of the controller design. Their values are selected via a PSO algorithm. The optimized waveform of the nonlinear SHSF is presented in the next section.

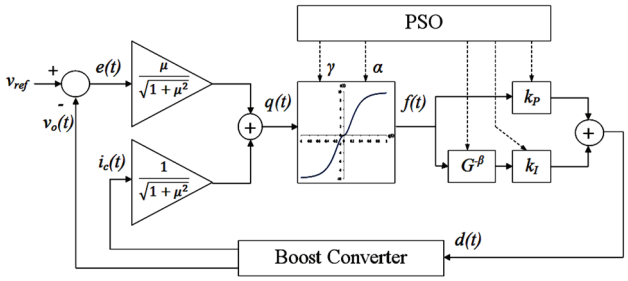


Fig. 2. Nonlinear Fractional-order PI (N-FoPI) control scheme.

The transition of the SHSF waveform offers favorable characteristics to achieve desired control objectives. It attenuates the modulated signal for extremely small values of *q(t)*. This feature improves damping to attenuate the oscillations, fluctuations and ripple in the steady-state response. The control surface exponentially enlarges the magnitude of *f(t)* when the value of *q(t)* increases. This feature aids in improving the transient-recovery response, error-convergence rate and disturbance-rejection capability of the system. Finally, the waveform tends to saturate at extremely large values of *q(t)*. This limiting phenomenon prevents the final control input *d(t)*. and the switching-transistor from getting saturated due to integral wind-up. The control surface can be implemented in practical systems, as shown in Section VI, since it does not put any recursive computational burden on the embedded control system. With the addition of a pre-stage nonlinear error modulator, the resulting Nonlinear-FoPI (N-FoPI) control law is given by Equ. (23).

$$d(t) = k_P . f(t) + k_I . \left(G^{-\beta} f(t)\right) \quad (23)$$

A block diagram of the N-FoPI control law is shown in Fig. 2.

## V. Particle Swarm Optimization

A PSO algorithm is a meta-heuristic computational optimization technique that involves the iterative improvement of candidate solutions with respect to a given performance index. It was inspired by the social behavior of bird flock [44]. This stochastic algorithm initializes with a randomly selected population of candidate solutions, denoted as 'particles'. It then explores and exploits the entire space to search for the global best-fit solution. The movement of each particle across the search-space is characterized by its position and velocity. The mathematic formulae of the velocity ($U_i$) and position ($X_i$) of the $i^{th}$ particle for the $j^{th}$ iteration are given in Equ. (24) and (25), respectively.

$$U_i^{j+1} = m_i U_i^j + f_1 b_1 \left(P_i - X_i^j\right) + f_2 b_2 \left(P_g - X_i^j\right) \quad (24)$$

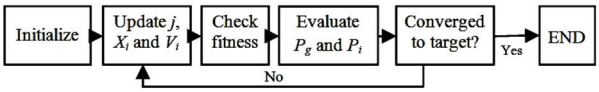


Fig. 3. PSO flow-chart.

$$X_i^{j+1} = X_i^j + U_i^j \tag{25}$$

where $f_1$ and $f_2$ are the cognitive-coefficients, $b_1$ and $b_2$ are random real-numbers between 0 and 1, and $m$ is the inertia-weight. Each of the cognitive coefficients has been assigned an equal value of 2.05 in order to make their sum greater than 4. The fitness value for each of the particles is computed, recorded and compared with the existing best-fit particles, also known as the "local-best" ($P_i$). The particle with the highest recorded value is selected as the new value of $P_i$. The particle with best fitness value among all of the particles in the population is chosen as the "global-best" ($P_g$). The convergence of the swarm depends on the value of $m$. This value balances the global and local searching capability of the optimization process. A higher $m$ offers good global search capability but a weak local search capability, and vice versa. Hence, in the beginning of a trial, a large value of $m$ is chosen to conduct the global searching. As the search progresses, the value of $m$ is reduced to support local searching. In this paper, the value of $m$ is iteratively updated according to the nonlinear function given in Equ. (26), [45].

$$m^j = m_{min} + (m_{max} - m_{min}).\left(\frac{j_{max} - j}{j_{max} - 1}\right)^y \tag{26}$$

where $j_{max}$ is the maximum number of iterations, and $y$ is the nonlinear-index number. Normally, the value of $y$ is set to 1.5 for the best performance of the optimizer [45]. The values of $m_{min}$ and $m_{min}$ are set to 0.4 and 0.9, respectively [45]. The value of $j_{max}$ in this paper is 100. The flow of the PSO algorithm is illustrated in Fig. 4. The algorithm iteratively computes and records the fitness of the particles using the quadratic performance index given in Equ. (27).

$$J = (t_s)^2 + (M_p)^2 + \int_0^t \tau e^2(\tau) + 0.1d^2(\tau)\, d\tau \tag{27}$$

The objective function in Equ. 27 is used to minimize the settling time ($t_s$), the peak overshoot ($M_p$), the integral of the time-weighted square-of-error, and the control signal ($d$) of the system in order to render optimality in both its transient-state and steady-state, and to control the energy expenditure. The fitness of each parameter is iteratively checked to determine its convergence to the $P_g$ value. The flow of the PSO algorithm is shown in Fig. 3.

The PSO algorithm is employed for the offline optimization of $k_P$, $k_I$, $\beta$, $\alpha$ and $\gamma$ by applying a step input. Initially, $k_P$ and $k_I$ are selected for the PI controller via a PSO. The fractional order $\beta$ is then optimized for the FoPI controller. Finally, $\alpha$ and $\gamma$ are tuned for the N-FoPI controller using a PSO algorithm. A population of 100 particles is selected for each of the parameters. The parameter optimization is summarized in Table II. The optimization history is illustrated in Fig. 4. The optimized SHSF waveform is depicted in Fig. 5.

TABLE II
OPTIMIZED VALUES OF THE PARAMETERS

| Parameter | $k_P$ | $k_I$ | $\beta$ | $\gamma$ | $\alpha$ |
|---|---|---|---|---|---|
| Value | 0.014 | 1.85 | 0.92 | 5.4 | 9.8 |
| Range | [0, 0.1] | [0, 10] | [0, 2] | [0, 10] | [0, 20] |
| Iterations | 92 | 81 | 68 | 80 | 86 |

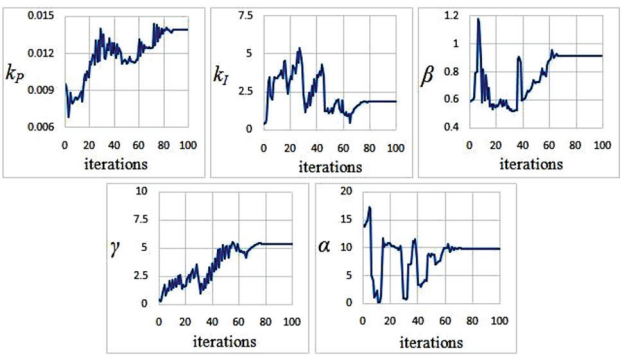


Fig. 4. Iterative optimization history.

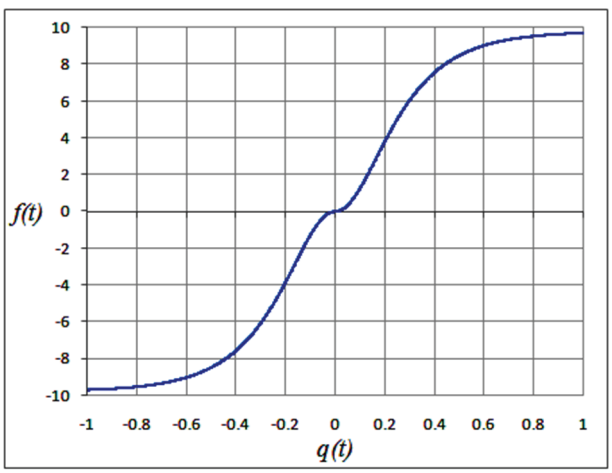


Fig. 5. Waveform of the signed hyperbolic secant function.

## VI. EXPERIMENTAL EVALUATION

This section presents details of both the hardware setup of the boost converter and the experimental analysis conducted on it to examine and validate the proposed control strategy.

### A. Experimental Setup

The hardware setup of the boost converter used in this paper is shown in Fig. 6. The analog measurements of $i_C$ are done via a current-sensing power resistor with a value of 0.01Ω (less than the capacitor's ESR). Analog measurements of $v_{in}$ and $v_o$ are done via dedicated potential-divider circuits. Raw analog sensor measurements are acquired via an 8-bit embedded microcontroller at a sampling frequency of 4.0 kHz.

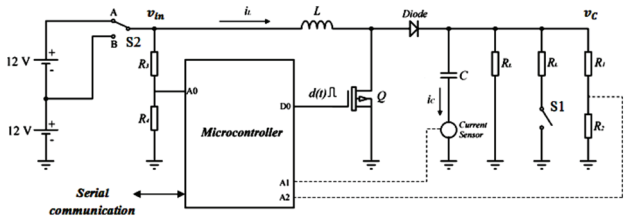


Fig. 6. Block diagram of the experimental setup.

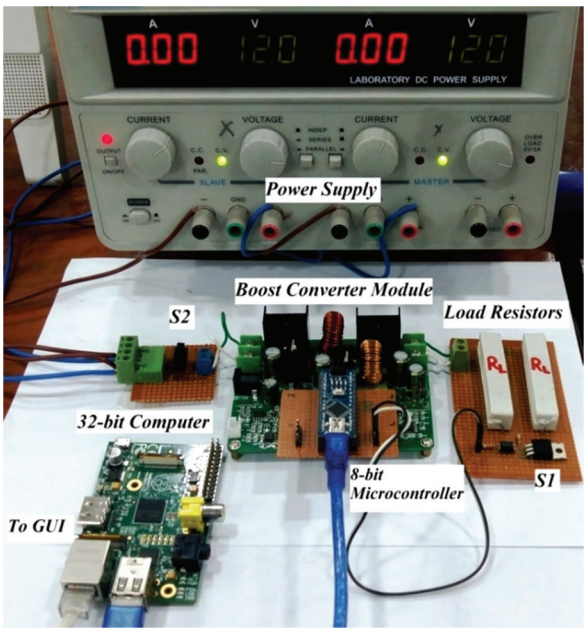


Fig. 7. Actual hardware setup.

The microcontroller filters outlier data from the sensor measurements and serially transmits the digitized sensor measurements to the feedback control routine running on a dedicated 32-bit computer with a 900 MHz clock speed [46]. Additionally, the computer is also responsible for running a LabVIEW based computer application for the sake of recording and graphically visualizing variations in the state-trajectories in real-time [47]. The control commands generated by the control routine are serially transmitted back to the microcontroller where they are transformed into equivalent high-frequency pulse-width-modulated (PWM) signals. The serial communication between the computer and the microcontroller is done at 9600 bps. These PWM signals are applied at the gate of the switching transistor ($Q$) via a dedicated optical isolation and a driver circuit.

The boost converter module is powered by a +24.0 V input source, which is supplied by serially connecting two individual +12.0 V supply outputs, using a variable dual-output lab-bench DC power supply. However, the input to the converter can be changed from +24.0 V to +12.0 using the switch S2 as shown in Fig. 6. This switching mechanism introduces step variations into the input voltage. This aids in testing the controller's ability to compensate the impact of rapid parametric variations. The load-resistance module of the circuit is made by connecting two fixed resistors, of equal values ($R_L$), in parallel with one another. One of the resistors is kept fixed. The other resistor can be included in or excluded from the circuit by simply turning-on or turning-off the switch S1. This switching mechanism introduces load- step transients into the overall circuit. This aids in examining the controller's robustness against impulsive disturbances caused by modeling errors. The voltage-dividers formed by $R_1$-$R_2$ and $R_3$-$R_4$ are used to monitor the variations in $v_o$ and $v_{in}$, respectively. The values of $R_1$ = 150 kΩ, $R_2$ = 1.0 MΩ, $R_3$ = 150 kΩ and $R_4$ = 750 kΩ. The analog measurements are fed to the 10-bit analog channels (A0, A1 and A2) of the 8-bit microcontroller. The PWM commands are generated by the digital pin (D0) of the microcontroller. A snapshot of the actual experimental setup is shown in Fig. 7.

### *B. Tests and Results*

The closed-loop time-domain performance of the N-FoPI controller is compared with those of PI and FoPI controllers through the following 'hardware-in-the-loop' experiments.

*1) Step-Reference Tracking*: This test examines the controller's ability to accurately track and regulate the $v_o$ of the boost converter at a desired reference of +30.0 V DC for a +24.0 V input. The switch S1, shown in Fig. 6, is kept "off" in all of the test trials. The corresponding time-domain responses of $v_o$, under the influence of each of the controllers, are shown in Fig. 8, 9 and 10.

*2) Load-Transient Recovery*: The impulsive disturbance rejection capability for each of the controllers is tested by artificially introducing load-step transients in the steady-state response of $v_o$ by turning on the switch S1 at t ≈ 0.39 s and turning it off again at t = 0.75 s, as discussed in Section VI A. This phenomenon leads to a step decrement followed by a step increment in the load resistance of the circuit. The resulting transients for each of the controlled systems, exhibited in the response of $v_o$, are illustrated in Fig. 11, 12 and 13.

*3) Input-Fluctuation Compensation*: In this test case, the robustness of each of the controllers in terms of compensating the influence of step fluctuations in the supply voltage is evaluated. For this purpose, the DC input voltage signal is artificially decreased from +24.0 V to +12.0 V by changing the position of the switch S2, shown in Fig. 6, from A to B. The corresponding variations for each of the controlled systems, exhibited in the response of $v_o$, are shown in Fig. 14, 15 and 16.

The responses are analyzed by evaluating their rise-time ($t_r$), over-shoot (OS), under-shoot (US), settling time ($t_s$) and root-mean-square of the steady-state error ($E_{ss}$). The test results are summarized in Table III. A comparative assessment clearly validates the efficacy and superior robustness of the N-FoPI control scheme. The PI controlled responses exhibit the slowest

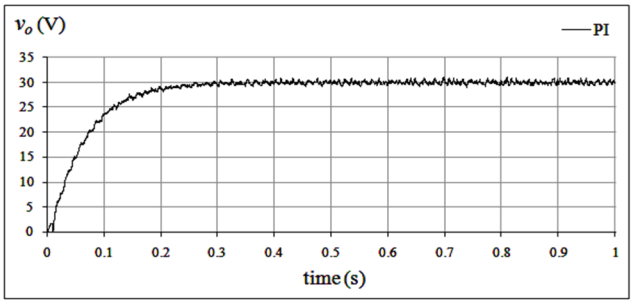

Fig. 8. Step reference tracking response of a PI controller.

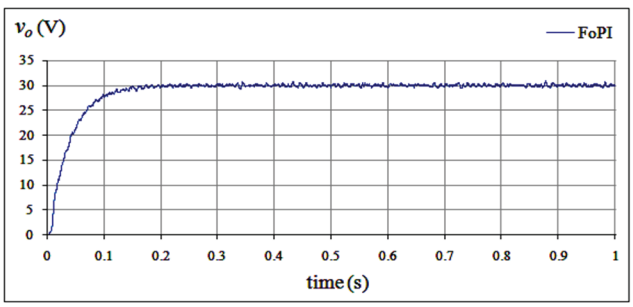

Fig. 9. Step reference tracking response of a FoPI controller.

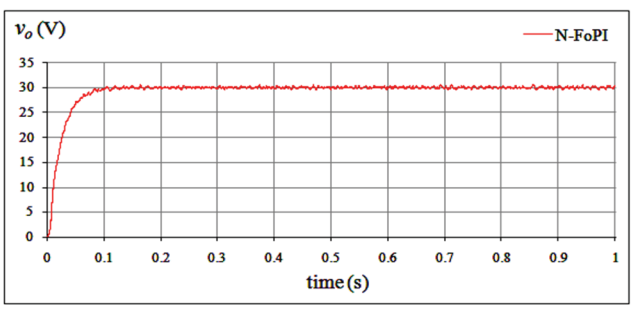

Fig. 10. Step reference tracking response of a N-FoPI controller.

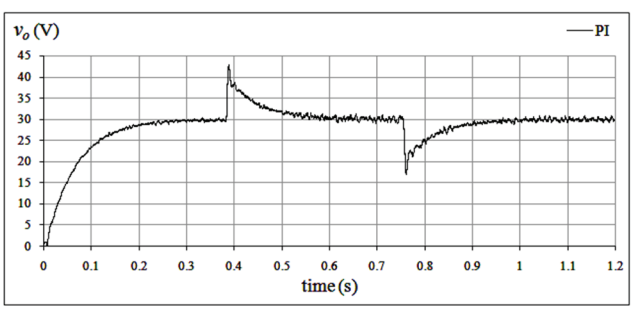

Fig. 11. Response of a PI controller under load-transients.

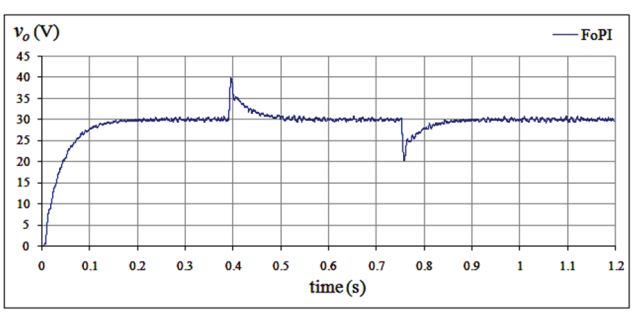

Fig. 12. Step response of a FoPI controller under load-transients.

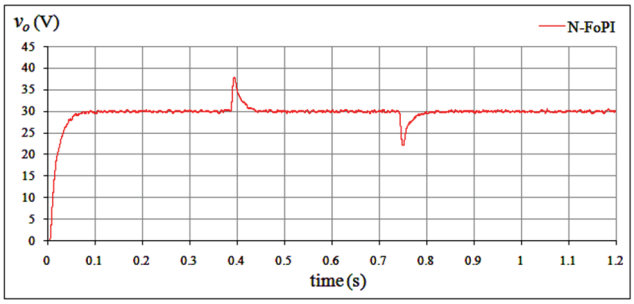

Fig. 13. Response of a N-FoPI controller under load-transients.

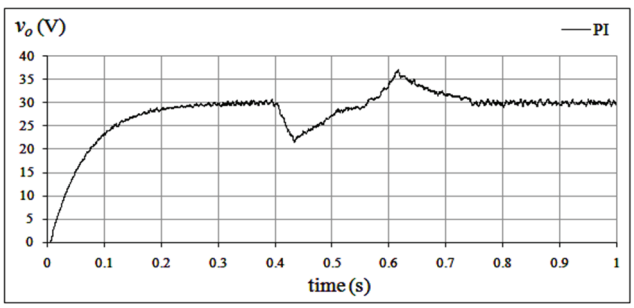

Fig. 14. Response of a PI controller under a $v_{in}$ fluctuation.

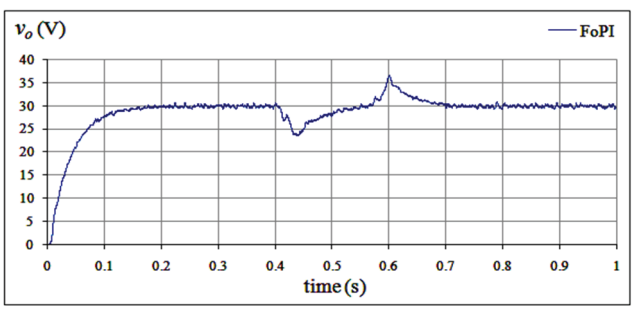

Fig. 15. Response of a FoPI controller under a $v_{in}$ fluctuation.

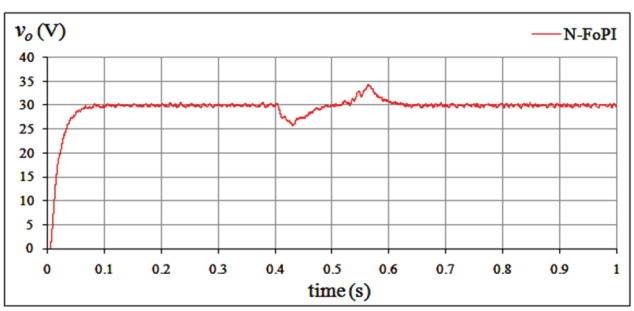

Fig. 16. Response of a N-FoPI controller under a $v_{in}$ fluctuation.

convergence rate and the poorest disturbance rejection capability. Its response takes the maximum transient recovery time with substantial oscillations. The FoPI controlled responses show a considerable improvement over the PI controlled responses by reducing the transitional times during transient recovery. The overshoots and undershoots are relatively smaller. Furthermore, it attenuates the oscillations as well as the steady-state fluctuations in the response. The N-FoPI controlled system yields the most time-optimal responses. Its response exhibits rapid transits with negligible

TABLE III
SUMMARY OF TEST RESULTS

| Controller → | | PI | FoPI | N-FoPI |
|---|---|---|---|---|
| Test A | $t_{rise}$ (ms) | 149.8 | 89.3 | 53 |
| | $t_s$ (ms) | 222.8 | 137.5 | 72.8 |
| | $E_{ss}$ (mV) | 8.24 | 6.89 | 4.51 |
| Test B | OS (V) | 12.89 | 9.92 | 7.68 |
| | US (V) | 13.01 | 9.83 | 7.71 |
| | $t_s$ (ms) | 183 | 116 | 53.5 |
| Test C | OS (V) | 7.04 | 6.66 | 4.36 |
| | US (V) | 8.51 | 6.44 | 4.22 |
| | $t_s$ (ms) | 342 | 296 | 209 |

oscillations. The ripple content is minimal when compared to the responses of the aforementioned controllers. Owing to the augmentation of the nonlinear error modulator, the controller takes the minimum time to recover from transients and settle at the reference voltage. It effectively damps overshoots and undershoots. As a result, it exhibits the minimum $E_{ss}$.

## VII. CONCLUSIONS

This paper presents a methodic approach to synthesize a robust and time-optimal output-voltage control strategy for DC-DC boost converters. The FoPI controller is at the heart of the proposed strategy.

The integration of fractional calculus with the conventional PI controller enhances the design flexibility. Apart from effectively eliminating the steady-state fluctuations and minimizing the ripple content in $v_o$, it enables systems to compensate for the un-modeled nonlinearities associated with complex dynamical systems. To further improve the controller's time-optimality, the FoPI controller is augmented with an SHSF-based error modulator that depends on variations in the error and $i_c$. The proposed augmentation enhances the controller's robustness against exogenous disturbances and unprecedented parametric variations. It enables the controller to compensate for the intrinsic nonlinearities associated with the system. Furthermore, the controller improves the overall transient recovery response of the system. The response exhibits a faster convergence rate while maintaining reasonable damping to suppress overshoots, undershoots and oscillations upon convergence. The aforementioned propositions are verified by conducting hardware-in-the-loop experiments on a 250W DC-DC boost converter prototype. In the future, a nonlinear error modulator will be constructed using neuro-fuzzy adaptation schemes. Other meta-heuristic computational methods will be investigated to optimize the controller parameters. The efficacy of the proposed control strategy will be analyzed by implementing it on other power electronic converters such as Cuk, SEPIC, Zeta, etc.

## REFERENCES


[1] P. Akter, M. Uddin, S. Mekhilef, N. M. L. Tan, and H. Akagi, "Model predictive control of bidirectional isolated DC–DC converter for energy conversion system," *Int. J. Electron.*, Vol. 102, No. 8, pp. 1407-1427, Aug. 2015.

[2] S. Sivakumar, M. JagabarSathik, P. S. Manoj, and G. Sundararajan, "An assessment on performance of DC-DC converters for renewable energy applications," *Renew. Sustain. Energy Rev.*, Vol. 58, pp. 1475-1485, May 2016.

[3] B. S. Lee, S. K. Kim, J. H. Park, and K. B. Lee, "Adaptive output voltage tracking controller for uncertain DC/DC boost converter," *Int. J. Electron.*, Vol. 103, No. 6, pp. 1002-1017, Jun. 2016.

[4] W. J. Lambert, R. Ayyanar, and S. Chickamenahalli, "Fast load transient regulation of low-voltage converters with the low-voltage transient processor," *IEEE Trans. Power Electron.*, Vol. 24, No. 7, pp. 1839-1854, Jul. 2009.

[5] H. Cui, J. Yang, and S. Li, "Nonlinear disturbance rejection control for a buck-boost converter with load uncertainties," in *Proc. 33rd IEEE CCC,* pp. 3788-3793, 2014.

[6] A. Ghosh and S. Banerjee, "Control of switched-mode boost converter by using classical and optimized type controllers," *Contr. Eng. Applied Informat.*, Vol. 17, No. 4, pp. 114-125, Dec. 2015.

[7] M. Hejri and H. Mokhtari, "Hybrid predictive control of a DC–DC boost converter in both continuous and discontinuous current modes of operation," *Optimal Contr. Appl. Methods*, Vol. 32, No. 3, pp. 270-284, May/Jun. 2011.

[8] M. Z. Hossain, N. A. Rahim, and J. Selvaraj, "Recent progress and development on power DC-DC converter topology, control, design and applications: A review," *Renew. Sustain. Energy Rev.*, Vol. 81, No. 1, pp. 205-230, Jan. 2018.

[9] S. Mariethoz, S. Almer, M. Baja, A. G. Beccuti, D. Patino, A. Wernrud, Buisson, J. H. Cormerais, T. Geyer, H. Fujioka, U. T. Jonsson, C. Y. Kao, M. Morari, G. Papafotiou, A. Rantzer, and P. Riedinger, "Comparison of hybrid control techniques for buck and boost DC-DC converters," *IEEE Trans. Contr. Syst. Technol.*, Vol. 18, No. 5, pp. 1126-1145, May 2010.

[10] L. Guo, J. Y. Hung, and R. M. Nelms, "Evaluation of DSP-based PID and fuzzy controllers for DC-DC converters," *IEEE Trans. Ind. Electron.*, Vol. 56, No. 6, pp. 2237-2248, Jun. 2009.

[11] K. Vijayakumar and T. Manigandan, "Nonlinear PID controller parameter optimization using enhanced genetic algorithm for nonlinear control system," *Contr. Eng. Applied Informat.*, Vol. 18, No. 2, pp. 3-10, Jun. 2016.

[12] P. Dobra, M. Trusca, D. Moga, and D. Petreus, "Stability aspects in DC-DC converters using PID controller," *Contr. Eng. Applied Informat.*, Vol. 9, No. 1, pp. 33-40, Mar. 2007.

[13] S. W. Seo, J. S. Park, Y. Kim, and H. H. Choi, "Fuzzy PI-type controller design for boost converter," *Int. J. Electron.*, Vol. 104, No. 1, pp. 143-156, Jan. 2017.

[14] Z. Salam, F. Taeed, and S. M. Ayob, "Design and implementation of a single input fuzzy logic controller for boost converters," *J. Power Electron.*, Vol. 11, No. 4, pp. 543-550, Jul. 2011.

[15] A. Kessal, L. Rahmani, J. P. Gaubert, and M. Mostefai, "Experimental design of a fuzzy controller for improving power factor of boost rectifier," *Int. J. Electron.*, Vol. 99,

No. 12, pp. 1611-1621, Dec. 2012.
[16] C. Olalla, I. Queinnec, R. Leyva, and A. E. Aroudi, "Robust optimal control of bilinear DC-DC converters," *Contr. Eng. Practice*, Vol. 19, No. 7, pp. 688-699, Jul. 2011.
[17] S. Singh, D. Fulwani, and V. Kumar, "Robust sliding-mode control of dc/dc boost converter feeding a constant power load," *IET Power Electron.*, Vol. 8, No. 7, pp. 1230-1237, Jul. 2015.
[18] A. Leon-Masich, H. Valderrama-Blavi, J. M. Bosque-Moncusí, J. Maixé-Altés, and L. Martínez-Salamero, "Sliding-mode-control-based boost converter for high-voltage–low-power applications," *IEEE Trans. Ind. Electron.*, Vol. 62, No. 1, pp. 229-237, Jan. 2015.
[19] V. Utkin and H. Lee, "Chattering problem in sliding mode control systems," in *Proc. IEEE VSS*, pp. 346-350, 2006.
[20] A. Amirahmadi, M. Rafiei, K. Tehrani, G. Griva, and I. Batarseh, "Optimum design of integer and fractional-order PID controllers for boost converter using SPEA look-up tables," *J. Power Electron.*, Vol. 15, No. 1, pp. 160-176, Jan. 2015.
[21] Z. Bingul and O. Karahan, "Comparison of PID and FOPID controllers tuned by PSO and ABC algorithms for unstable and integrating systems with time delay," *Optimal Contr. Appl. Methods*, Vol. 39, No. 4, pp. 1431-1450, Jul./ Aug. 2018.
[22] K. A. Tehrani, A. Amirahmadi, S. M. R. Rafiei, G. Griva, L. Barrandon, M. Hamzaoui, I. Rasoanarivo, and F. M. Sargos, "Design of fractional order PID controller for boost converter based on Multi-Objective optimization," in *Proc. 14th IEEE PEMC*, T3-179 - T3-185, 2010.
[23] S. K. Verma, S. Yadav, and S. K. Nagar, "Fractional order PI controller design for non-monotonic phase systems," *IFAC-PapersOnLine*, Vol. 49, No. 1, pp. 236-240, 2016.
[24] G. E. Pitel and P. T. Krein, "Minimum-time transient recovery for DC–DC converters using raster control surfaces," *IEEE Trans. Power Electron.*, Vol. 24, No. 12, pp. 2692-2703, Dec. 2009.
[25] S. Kapat and P. T. Krein, "Formulation of PID control for DC–DC converters based on capacitor current: A geometric context," *IEEE Trans. Power Electron.*, Vol. 27, No. 3, pp. 1424-1432, Mar. 2012.
[26] J. B. L. Fermeiro, J. A. N. Pombo, M. R. A. Calado, and S. J. P. S. Mariano, "A new controller for DC-DC converters based on particle swarm optimization," *Applied Soft Computing*, Vol. 52, pp. 418-434, Mar. 2017.
[27] R. Senthilkumar and V. Manikandan, "Design of fractional order PI controller using metaheuristic algorithms applied to DC-DC boost converter - A comparision," *ARPN J. Eng. Applied Sci.*, Vol. 10, No. 11, pp. 4832-4837, Jun. 2015.
[28] M. H. Rashid, Power Electronics: Circuits, Devices, and Applications, Pearson Education, 2009.
[29] M .M. Peretz and S. B. Yaakov, "Time-domain design of digital compensators for PWM DC-DC converters," *IEEE Trans. Power Electron.*, Vol. 27, No. 1, pp. 284-293, Jan. 2012.
[30] R. Priewasser, M. Agostinelli, C. Unterrieder, S. Marsili, and M. Huemer, "Modeling, control, and implementation of DC–DC converters for variable frequency operation," *IEEE Trans. Power Electron.*, Vol. 29, No. 1, pp. 287-301, Jan. 2014.
[31] S. Padmanaban, E. Kabalci, A. Iqbal, H. Abu-Rub, and O. Ojo, "Control strategy and hardware implementation for DC-DC boost power circuit based on proportional-integral compensator for high voltage application," *Eng., Sci. Tech.*, Vol. 18, pp. 163-170, Jun. 2015.
[32] A. T. Azar, A. G. Radwan, and S. Vaidyanathan, Fractional Order Systems: Optimization, Control, Circuit Realizations and Applications, Elsevier Science & Technology, 2018.
[33] A. Tepljakov, Fractional-order Modeling and Control of Dynamic Systems, Springer; 2017.
[34] M. A. Rahimian, and M. S. Tavazoei, "Improving integral square error performance with implementable fractional-order PI controllers," *Optimal Contr. Appl. Methods*, Vol. 35, No. 3, pp. 303-323, May/Jun. 2013.
[35] M. Zamani, M. Karimi-Ghartemani, and N. Sadati, "FOPID controller design for robust performance using particle swarm optimization," *J. Fractional Calculus Applied Analysis*, Vol. 10, No. 2, pp. 169-188, 2007.
[36] R. Kelly and R. Carelli, "A class of nonlinear PD-type controller for robot manipulator," *J. Robotic Syst.*, Vol. 13, No. 12, pp. 793-802, Dec. 1996.
[37] Y. Xu, J. M. Hollerbach, and D. Ma, "A nonlinear PD controller for force and contact transient control," *IEEE Control Syst. Mag.*, Vol. 15, No. 1, pp. 15-21, Mar. 1995.
[38] H. Seraji, "A new class of nonlinear PID controllers with robotic applications," *J. Robotic Syst.*, Vol. 15, No. 3, pp. 161-181, Mar. 1998.
[39] L. Corradini, A. Babazadeh, A. Bjeletic, and D. Maksimovic, "Current-limited time-optimal response in digitally controlled DC–DC converters," *IEEE Trans. Power Electron.*, Vol. 25, No. 11, pp. 2869-2880, Dec. 2010.
[40] S. Kapat and P. T. Krein, "Improved time optimal control of a buck converter based on capacitor current," *IEEE Trans. Power Electron.*, Vol. 27, No. 3, pp. 1444-1454, Mar. 2012.
[41] Z. Salam, F. Taeed, and S. M. Ayob, "Design and implementation of a single input fuzzy logic controller for boost converters," *J. Power Electron.*, Vol. 11, No. 4, pp. 542-550, Jan. 2011.
[42] F. Taeed, Z. Salam, and S. Ayob, "FPGA implementation of a single-input fuzzy logic controller for boost converter with the absence of an external analog-to-digital converter," *IEEE Trans. Ind. Electron.*, Vol. 59, No. 2, pp. 1208-1217, Feb. 2012.
[43] S. M. Ayob, N. A. Azli, and Z. Salam, "PWM DC-AC converter regulation using a multi-loop single input fuzzy PI controller," *J. Power Electron.*, Vol. 9, No. 1, pp. 124-131, Jan. 2009.
[44] E. Sahin and I. H. Altas, "A PSO tuned fractional-order PID controlled non-inverting buck-boost converter for a wave/UC energy system," *Int. J. Intelligent Syst. Appl. Eng.*, Vol. 4, pp. 32-37, Dec. 2016.
[45] A. Djoewahir, K. Tanaka, and S. Nakashima, "Adaptive PSO-based self-tuning PID controller for ultrasonic motor," *Int. J. Innovative Comput., Informt. Contr.*, Vol. 9, No. 10, pp. 3903-3914, Jan. 2013.
[46] M. Boutouba, A. El-Ougli, S. Miqoi, and B. Tidhaf, "Intelligent control for voltage regulation system via DC-DC converter using raspberry Pi 2 board," *WSEAS Trans. Electron.*, Vol. 8, pp. 41-47, 2017
[47] M. Demirtas and G. Gezer, "Analyzing of PI controlled DC/DC converter output voltage using LABVIEW," in *Proc. 18th IEEE SIU*, pp. 704-707, 2010.

**Omer Saleem** received his B.S. and M.S. degrees in Electrical Engineering with a specialization in control systems from the University of Engineering and Technology, Lahore, Pakistan. He is presently working as an Assistant Professor in the Department of Electrical Engineering, National University of Computer and Emerging Sciences (NUCES), Lahore, Pakistan. He has published several research papers in highly indexed journals. His current research interests include the adaptive and optimal control of electrical energy conversion systems and under-actuated mechatronic systems.

**Mohsin Rizwan** received his B.S. degree from the Department of Mechanical Engineering, University of Engineering and Technology (UET), Lahore, Pakistan; and his Ph.D. degree from the University of Texas at Arlington, Arlington, TX, USA, in 2011. He is presently working as an Assistant Professor in the Department of Mechatronics and Control Engineering, UET. His current research interests include system modeling, MEMS, and the design and analysis of feedback control systems.

**Ahmad Khizar** received his B.S. degree in Electrical Engineering with a specialization in power systems from the University of Lahore, Lahore, Pakistan; and his M.S. degree in Mechatronics and Control Engineering from the University of Engineering and Technology (UET), Lahore, Pakistan. He is presently working as an Assistant Manager in the National Engineering Services Pakistan (NESPAK), Lahore, Pakistan. His current research interests include HVS design and advanced hybrid energy systems.

**Muaaz Ahmad** received his B.S. degree in Electrical Engineering with a specialization in computers from the National University of Computer and Emerging Sciences (NUCES), Lahore, Pakistan. He is presently working as a Software Consultant at Zortik Technologies, Lahore, Pakistan. His current research interests include embedded computing, microprocessor-based automation, embedded robotics and computational optimization. He is an active Member of the IEEE.